Bifacial Schottky-Junction Plasmonic-based Solar Cell

M. Farhat[a], A. A. B. Baloch[b], S. N. Rashkeev[b], N. Tabet[c], S. Kais[d], F. H. Alharbi[e,f,*]

[a] *Department of Electrical Engineering, King Abdullah University of Science and Technology (KAUST), Saudi Arabia*

[b] *Qatar Environment & Energy Research Institute (QEERI), Hamad Bin Khalifa University, Doha, Qatar*

[c] *Department of Applied Physics and Astronomy, University of Sharjah, UAE*

[d] *Department of Chemistry, Department of Physics and Birck Nanotechnology Center, Purdue University, West Lafayette, IN USA.*

[e] *Department of Electrical Engineering, King Fahd University of Petroleum and Minerals, Dhahran, Saudi Arabia.*

[f] *K.A.CARE Energy Research & Innovation Center, Dhahran, Saudi Arabia.*

Abstract

Plasmonically-enhanced and Schottky-based devices are very appealing candidates for sunlight energy-harvesting applications. However, this class of structures introduces inherent limitations such as thermionic emission (and the related dark current). In this paper, we theoretically propose to use the metal-semiconductor-metal heterojunction under bifacial mode. In this design, plasmonic periodic gratings are introduced in the bifacial configuration to allow

This article has been accepted for publication and undergone full peer review but has not been through the copyediting, typesetting, pagination and proofreading process, which may lead to differences between this version and the Version of Record. Please cite this article as doi: 10.1002/ente.201901280.

collection of light from both faces of the solar junction. This results in an improved carrier generation and enhanced device performance of a cell with 3 μ m-thick Si absorber. Bifacial gain for short circuit current was found to be 88%. with a bifaciality factor (the ratio of rear to front response of the device) of 84%. By optimizing the filling fractions of front and rear plasmonic gratings, the obtained normalized output was able to become higher than 25%, i.e., it almost doubles the performance with the monofacial Schottky solar cell.

Keywords: Plasmonics, Schottky, Bifacial, Photovoltaic, Optoelectronic

*Corresponding author *Email address:* fahhad.alharbi@kfupm.edu.sa (F. H. Alharbi)

1. Introduction

With a continuous global growth and industrial development, the needs and requests for energy have reached unprecedented levels and may become unsustainable[1,2] as the conventional finite energy-reserves are being drained at an alarming rate. In fact, it is believed that the production of oil has peaked and it will start declining in a decade or so[3,4] while the production of uranium would peak as well in two decades[5]. Thus, there is a vital necessity to find new sources of energy. Undoubtedly, solar energy is considered among the main compelling alternatives to solve this crisis. For this reason, the research and development of solar cells has evolved remarkably and in numerous fronts over the past decade. Besides the economical factor, the field has been taking advantage from the exponential advances in nanotechnology and material sciences[6,7]. As known, solar cell technologies rely heavily on the choice of proper materials.

Historically, the first ever successful fabrication of a Solar Cell (SC) was achieved in the 1950s[8,9], where it was primarily based on Silicon (Si). Then in the 1970s, a huge set of inorganic absorbers were considered to make cells that are more efficient. The most prominent technologies

that originated from these activities are cadmium telluride (CdTe) and copper indium gallium selenide (CIGS)[9] solar cells. Since then, the space of absorbers has been expanding[10]. The most noticeable development in the recent years is the emergence of a family of hybrid perovskites solar cells. In just few years since they were first proposed (in 2009[11]), their efficiency surpassed the commercialization demarcation line and reached the 25.2% level[12]. However, there are other outstanding challenges associated with their stability and toxicity[13,14].

As aforementioned, photovoltaics (PV) could thus be one possible solution to the increasing demand for energy[15,16]. However, before this comes to reality, there is a need to enhance the level of efficiency of actual solar cells (at least to 20%) and to reduce their cost to make it competitive in energy market. Plasmonic metamaterials could lift some of the present issues by offering the potential to design man-made nano-structured systems with optical characteristics that are optimized to respond in solar radiation spectral region[17–22]. This field of research targets investigating the intriguing optical properties of two-dimensional (2D) and three-dimensional (3D) nano-structures, resulting from surface plasmon polaritons modes (SPP)[23], that can lead to an improved light absorption (useful for designing solar cells with enhanced functionalities)[24–28]. Thus these plasmonic structures showed to be very useful for light energy harvesting purposes, e.g. thermal photovoltaics[29], thin film PV devices[30], or even thermoelectrics[31]. These functions rely on the ability of metamaterials and SPPs to focus light and thus to absorb more incoming energy[32,33,34].

In the same vein, Schottky-based solar cells can represent a viable alternative to p-n junction SC that rely on the diffusion of an impurity donor in a p-type substrate. On the contrary, Schottky-based solar cells need a single doped absorber layer as the junctions are formed with the contacts. This is a big advantage when it comes to the simplicity of fabrication and hence the cost. Furthermore, by proper design and light management, the required thickness of the absorber can be reduced considerably. This shall allow reducing the cost further due to the smaller needed materials

and also the enhanced tolerance to faults. In solar cells, both optical and electrical performances of the device must be maintained. If the needed electronic transport lengths got smaller, smaller electronic conductivity would be required and hence the film quality could be tolerated.[22,35–40]. Several approaches have been proposed in the recent years to exploit this class of PV cells, by exploiting, for instance, the use of plasmonic designs that results in an enhancement of the efficiency[19–22].

In this work, we explore the deployment of plasmonic and nanophotonic structures in bifacial modes, such as metamaterials, in order to realize cost-effective designs of SC with high-energy generation[22]. In particular, one interesting avenue to enhance the energy yield of Schottky PV cells, without considerably increasing the fabrication cost, is to use bifacial designs[41–43]. In principle, allowing light collection from both facets of the cell [See Figure 1(a)] can considerably enhance the rate of photo-generation and enhance J_{sc} (short-circuit current), resulting finally in a significant efficiency improvement[44–46]. Their performance is primarily dependent on the increase of generation current from rear side and bifaciality factor (ratio of rear to front current response). At the module level, an energy efficiency improvement of 54% by employing highly reflective albedo material has been demonstrated for regular bifacial SC[47]. On the other hand, bifacial cells coupled with plasmonic structures can further increase the light absorption capability, thereby, leading to high efficiency and consequently low-cost of energy. Considering the need, this study proposes a Schottky-junction solar cell using the synergistic effect of plasmonics and bifaciality through an opto-electronic device design.

2. Computational Methodology

Recent studies suggest the advantage of using a metal-semiconductor based design, the so-called Schottky-junction, as a basis for photovoltaic devices enhanced by the plasmonic effect[22]. These junctions consist of an active semi-conducting material (Silicon, for example) of n-

or p-type, sandwiched between two plates of metals with different work functions (e.g. gold and silver). A spatial charge zone is thus created at the interface between materials, resulting in a Schottky barrier of height Φ_B, as schematized in Figure 1(b). In this study, the used silicon is of n-type, so the height of the barrier is given by

$$\Phi_B = \phi_{m1} - \chi_{si} \tag{1}$$

where ϕ_{m1} is the work function of the top contact (gold) and χ_{si} is the electrical affinity of silicon. Additionally, the second (bottom) interface is characterized by the built-in potential, and in order to make ohmic contact, band alignment constraint must be satisfied by ensuring the following criteria

$$E_c - E_F > \phi_{m2} - \chi_{si}, \tag{2}$$

where ϕ_{m2} the work function of the bottom contact (silver), E_c and E_F represent the conduction and Fermi levels of silicon, respectively, as schematized in Figure 1(b).

This class of solar cells is well-known to possess mainly a minority and majority carrier current paths. The latter is specific for Schottky SC and originates from thermionic emission, which can result in lower voltages,

$$J = J_0(\exp(eV / k_B T) - 1). \tag{3}$$

where J is the current density across the junction, J_0 is the saturation current density, V is the voltage across the junction, k_B is the Boltzmann constant, and T is the temperature in Kelvin. These low voltages are thus detrimental to the net efficiencies of these cells. However, the use of Schottky cells can be justified by their ease of fabrication and fault tolerance as aforementioned (in comparison to p-n junction SC). This results consequently in the reduction of the production cost of the PV cell. Another important advantage of these cells is the possibility of designing them using the bifacial concept [See Figure 1(a)] by allowing collection of both direct light (upper interface) and albedo component (reflected and scattered light, at the lower interface). Moreover, the lower interface suffers from less accumulation of dust, in desert environment (where the energy irradiance

is the strongest and where the future power plants are more likely to be built). This allows for higher efficiency from the second face of the SC, and an increased yield of the overall cell.

To compute the optical profile in the cell due to solar irradiation, COMSOL Multiphysics computer codes were used[49]. A 2D periodic array of plasmonic meta-atoms (with periodicity of 1μ m) was considered, and Floquet periodicity was assumed in the x-direction (as can be seen in Fig. 1(a)). An impinging plane-wave with broad spectrum (300-1300 nm), polarized along the x-axis is used for the excitation of the structure. The optical properties of each material are extracted from experimental data[50,51] and COMSOL's interpolation algorithm is employed. The generation rate is integrated with respect to wavelength and plotted in Fig. 3(b). The convergence of each simulation is verified by convenient tailoring of the mesh.

For analyzing the electrical functioning of the bifacial Schottky SC, the J-V characteristic is computed using the Solar Cell Capacitance Simulator software (SCAPS). It is a one-dimensional (1D) drift-diffusion solver. To use it for higher dimensional structured systems, the carrier diffusion length must be higher than the scale of corrugation. If this condition is satisfied, carrier transport across the layers ($x-y$ plane) can be averaged and the 1D calculations are performed along the direction between the contacts (z-axis). For the studied system, this is the case as the routinely obtained diffusion length of electrons and holes in Si is around 200 μm[10] while the used grating is in μm scale. SCAPS solves the electrostatic equations with continuity conditions across the SC by taking the absorption and generation rate from the optical simulations.

That is

$$\frac{\partial n_p(z,t)}{\partial t} = -\frac{1}{q}\frac{\partial \mathbf{j}_p(z,t)}{\partial z} + \mathbf{G}(z) - \mathbf{U}(z),$$

$$\frac{\partial n_n(z,t)}{\partial t} = \frac{1}{q}\frac{\partial \mathbf{j}_n(z,t)}{\partial z} + \mathbf{G}(z) - \mathbf{U}(z), \tag{4}$$

$$\nabla\cdot(\epsilon\nabla\phi) = -\rho, \tag{5}$$

where ϵ, q are the permittivity of Si and electronic unit-charge, respectively. $\mathbf{G}(z)$ and $\mathbf{U}(z)$ are the averaged generation and recombination rates, respectively. The charge density is given by $\rho = q(n_n - n_p + N_A - N_D)$ where n_n, n_p, N_A, and N_D are the densities of electrons, holes, acceptor, and donor impurities. As we assume n-doped Si, we take $N_A = 0$, $N_D = 10^{16} cm^{-1}$. Due to the spatial reduction, ∇ is simply $\partial / \partial z$. Furthermore, the averaged current densities of electrons and holes are

$$\mathbf{j}_{n,p} = -q\mu_{n,p} n_{n,p} \pm qD_{n,p} \nabla n_{n,p} . \tag{6}$$

the total current is $\mathbf{j} = \mathbf{j}_n + \mathbf{j}_p$ and μ and D are the mobility and diffusion coefficients. The electrical parameters of the materials are assumed to be same as in Ref.[22]. The optical and electrical models are then coupled to form a mutli-physics model for bifacial schottky solar cell. This assists in analyzing the optical impact of grating geometry as well as the carrier generation and transport in the complete device.

The proposed cell's geometry is depicted in Figures. 1(a)-1(b). The cell is made of a central silicon layer sandwiched between two metallic gratings (gold on the top forming a Schottky barrier and silver on the bottom forming an ohmic contact). It is assumed that both metallic contacts are corrugated in a periodic manner [See Figure 1(a)] in the x-direction (with a period of $P_0 = 1 \ \mu$ m) to allow for SPP excitation at both facets of the cell. The design is assumed to be extended to infinity in the y-direction, but a periodicity in that direction could be created in a similar way. Based on the maximum absorption, thickness of the absorber was taken as, $t_0 = 3 \ \mu$ m. Here the electric field is polarized along the periodicity direction (x-direction). All optical parameters of the materials (semiconductor absorber and metallic contacts), i.e. their refractive index[50] and optical conductivity[51] are taken from available experimental data[48]. We assume that the parameters of the gratings such as the filling fractions ω_i / P_0 (changing in the range between δ and 1, where δ is a small parameter) and the heights h_i could be different, and are based on experimental capabilities[52].

3. Results and Discussion

3.1. Optical simulations

Figure 2(a) plots the experimental values of the extraterrestrial (ETR) spectral irradiance, and is compared to the one obtained using global tilt. These experimental data can be approximated by the spectral irradiance of a 5800 K black-body (Sun's surface temperature), described by

$$S_r = \left(\frac{R_s}{r_{se}}\right)^2 \frac{8\pi\hbar c}{\lambda^5}\left(\frac{1}{e^{\frac{\hbar c}{\lambda k_B T}} - 1}\right), \tag{7}$$

with R_s is the Sun's radius and r_{se} is the average distance between the Sun and the planet Earth [See Figure 2(a)], c is the speed of light, and λ is the wavelength. In the remainder of this study, we consider that our incident electromagnetic powers are approximated by Eq. (7).

The albedo of the surface is the ratio of the reflected light intensity to the total incoming solar radiation intensity. It has both directional and spectral dependence for any specific type of material[47]. Figure 2(b) shows the hemispherical spectral albedo of materials that are typical for PV installation environment such as grass, snow, sand dune, water and red bricks[48]. Albedo is the main parameter governing the rear side contribution of the bifacial SC which can alter the spectral response of the solar cells. Therefore, its analysis and impact on PV can assist in optimal selection of design parameters. The integrated average values of spectral albedo, in the range of $300 - 1300$ nm, varies from 0.15 for grass to 0.88 for snow. However, higher average values do not necessarily imply that a particular albedo will enhance the performance of the SC. It should also cover the spectral response of the solar cell being under investigation. Sand dune (with an average albedo coefficient of 0.72) and snow exhibit the best potential because of their high albedo coefficient and wide spectral range.

Figures 2(c)-(d) show the absorption spectra of the two plasmonic gratings [of Figure 1(a)] for different filling fractions ω_i / P_0. These graphs reveal that considerable enhancement of the absorption can be achieved for the two geometries of interest, especially when the filling fractions are equal to 0.5. However, by optimizing the geometry and the thickness of Si, and by adding a bottom metallic layer, it is possible to obtain total light absorption; this is the well-known perfect (coherent) absorption and is equivalent to the phenomena observed in laser techniques[53]. The electric field norm distribution $|\mathbf{E}(\mathbf{r},\lambda)|$ is displayed in Figure 2(e) and shows the characteristic of the excited dipole modes. It should be mentioned here that due to the 3 μ m-thickness of silicon layer, no coupling between the SPP modes at Au/Si and Ag/Si interfaces is allowed, and therefore the corresponding plasmonic fields are unhybridized.

The next step is to consider the underlying mechanism of the photo-generation in the silicon layer. The main physical parameter is the photo-generation rate (due to the incident light). To compute it, one should numerically calculate the portion of absorption by the plasmonic structures, using Maxwell equations $\nabla \times (\nabla \times \mathbf{E}(\mathbf{r},\lambda)) - k_0^2 \epsilon_r \mathbf{E}(\mathbf{r},\lambda) = \mathbf{0}$, (for example, by finite elements technique), using the wave optics module of the COMSOL codes[49]. Here, k_0 is free-space wave number and E is the frequency-dependent electric field. Then, by taking the divergence of the Poynting vector, one can calculate the energy absorption coefficient $Q_{abs}(\mathbf{r},\lambda)$, using electric field norm distribution $|\mathbf{E}(\mathbf{r},\lambda)|$ and imaginary part of Si permittivity $\mathrm{Im}(\epsilon(\lambda))$ such that

$$Q_{abs}(\mathbf{r},\lambda) = -2\pi \frac{\mathrm{Im}(\epsilon(\lambda))}{\lambda} |\mathbf{E}(\mathbf{r},\lambda)|^2 . \quad (8)$$

From Eq. (8), one can expect that higher absorption rate can be obtained from higher values of the electric field, confirming the idea behind this work, that consists in exploiting SPPs to enhance the efficiency of Schottky SC [See Figure 2(e)].

The next step is to relate Q_{abs} to the number of photo-generated electrons (and holes),

versus the position [shown in Figure 3(a)]. This is done by integrating over the wavelengths as follow

$$G(\mathbf{r}) = 2\int G_0(\mathbf{r},\lambda)\,d\lambda = 2\int Q_{abs}(\mathbf{r},\lambda)\frac{\lambda}{hc}d\lambda, \tag{9}$$

where $G_0(\mathbf{r},\lambda)$ and $G(\mathbf{r})$ represent the spectral photo-generation and an integrated one, respectively whereas hc/λ is the energy of photon. The factor of 2 accounts for the possibility of having electric current by a flow of electrons and another flow of holes. Figure 3(a) shows the integrated spatial $G(\mathbf{r})$, for wavelengths of the incoming light ranging from 300 nm to 1300 nm, versus the depth into the active absorber (silicon). At the beginning, we consider direct light shining on the gold grating, with the filling fraction $\omega_1 / P_0 = 0.5$ and height $h_1 = 50$ nm. These plots show the efficiency of using the plasmonic assistive grating, since most of wavelength components get absorbed within the relatively-low thickness of Silicon absorber i.e near metal-Si interface. This fact is straightforward for the blue components of the spectral irradiance, but for longer wavelengths (red-part) silicon is known to possess low absorption coefficient, which explains the large thickness of typical p-n silicon solar cells (in the 100 μ m range). In Figure 3(a), we plot the two-dimensional behavior of the photo-generation when direct light falls on the gold grating and when the representative sand albedo is incident on the silver grating with the same ω_i / P_0 and h_i. The last part of this plot gives the main result of this study, i.e. the total photo-generation rate when one allows light collection from both sides of the SC with two corrugated gratings, as described earlier. It is thus clearly seen in Figure 3(b) that $G(\mathbf{r})$ shows two peaks (with exponential decay) corresponding to the two interfaces (Si/Au and Si/Ag). The spectrally-integrated photo-generation rate is shown in Figure 3(b) along the thickness of absorber, and shows the expected quasi-exponential decay, when one moves away from the metal-Si interface. The photo-generation (and consequently the maximum short circuit-current $J_{sc} = \iiint G(\mathbf{r})d^3r$) is significantly enhanced thanks to the plasmonic effect (strong light absorption) as well as the bifacial operation (allowing more incoming power). It can be noticed that for the set of geometrical parameters that we use, the

photo-generation shows an asymmetric behavior (being larger at the gold interface side), because albedo intensity (from Ag side) is weaker than the direct light (from Au side).

3.2. Electrical simulations

Photovoltaic solar cells are mainly characterized by their efficiency i.e. the fraction of power (incoming from the sun) that they convert into the electric power. Bifacial SC are able to convert light from both sides, front and rear, whereas monofacial SC only harness the light from the front side. The useful albedo portion of the incoming light does not contribute to power generation in monofacial SC. Therefore, the normalized output η^* (output power normalized to one sun) is the total power produced by Schottky SC when incoming light from both front and rear sides is collected. This normalized output is given by

$$\eta^* = \frac{J_{sc} \cdot V_{oc} \cdot FF}{P_{inc}}, \tag{10}$$

where J_{sc} is the short-circuit current , V_{oc} is the open-circuit voltage, FF is the fill factor, and P_{inc} is incident power for one sun. Here J_{sc} is the total short-circuit current, that is generated by collecting light from both sides. It is the calculated area (highlighted in yellow) color in Figure 3(b).

The front side has as expected a higher J_{sc} relative to the rear-side illumination whereas the V_{oc} is almost unchanged as shown by Figure 4(a). The total (normalized bifaical) J - V characteristic is given for comparison and is slightly different from the addition of J_{sc} (of individual faces). This difference can be attributed to the increased built-in potential and drift force on carriers when we shine from both sides simultaneously i.e. the case of total (Normalized Bifacial). Whereas, by adding linearly the individual contribution of both faces, V_{oc} remains the same.

Figure 4(b) compares the quantum efficiency of the front and rear faces. Infrared spectral losses are found to be higher when illuminated from back (Ag-side) face of Schottky solar cell. The

main driving parameter for bifacial is the enhancement of J_{sc} from individual 25.54 mA/cm2 (front) and 21.57 mA/cm^2(rear) to 48.05 mA/cm2 for bifaical mode. It can be observed that the current density (photo-generation) exhibits an asymmetric behavior (higher at gold interface side with J_{sc}=25.54 mA/cm^2), because albedo radiation (from Ag side J_{sc}=21.57 mA/cm^2) is weaker than the front-side incoming irradiation at the Au side. Since the V_{oc} values are close to each other for all configurations, it implies comparable saturation current losses, therefore the FF does not drop when we move from monofacial (82.62% (front) and 82.53% (rear)) to bifaical device (82.9%). η^* was found to be 12.49% when illuminated from front(Au) side whereas it was reduced to 10.4% when shined from rear side (Ag). Consequently, the final bifacial Schottky design resulted in a normalized efficiency, η^*, of 24.26%.

To understand the asymmetric opto-electronic behavior of bifacial devices, it is important to introduce bifaciality factor and bifacial gain. Bifaciality factor (BF) is the quantification of the rear to front side response of the device. BF is shown by Eq. (8) and provides a measure of the relative performance of each side when illuminated separately. On the contrary, Bifacial gain (BG) signifies the additional contribution due to the rear side illumination as is defined as Eq. (9).

$$BF = \frac{X_{\text{rear}}}{X_{\text{front}}}, \tag{11}$$

$$BG = \frac{X_{\text{bifacial}} - X_{\text{front}}}{X_{\text{front}}}, \tag{12}$$

where x is any opto-electronic parameter of the device under front, rear and bifacial illumination mode.

Figure 5 highlights the BF and BG of electrical parameters obtained from device simulations. BF is shown in Figure 5(a) where it can be seen that V_{oc} and FF retain values of 99%

and 100% implying that the rear side performs similar to the front side. Also, it can be deduced that the device does not undergo additional losses when shined from rear side due to higher BF. Short circuit current, J_{sc}, has a BF of 84% which is primarily due to less absorption of light and hence photo-generated carriers from the rear side albedo illumination. Correspondingly,bifaciality factor of efficiency was found to be 84%. On the other hand, Figure 5(b) shows that the main gain was due to current generation. BG for J_{sc} was found to be 88% by designing the proposed Schottky cell architecture and introducing plasmonic gratings.

3.3. Geometric Simulations

A parametric study based on filling fractions of front and rear contacts was carried out to analyze the optimal geometry. Figure 6 shows the normalized output with one sun illumination, η^*, of the solar cell as a function of filling fraction of the gratings (ω_i / P_0, i=1,2). The regions depicted with blue color correspond to lower values of η^* (while the region red color correspond to high η^*). From this graph, it can be easily inferred that values of ω_i / P_0 around 0.5 corresponds the best for high conversion efficiency. The white star has coordinates (0.5, 0.5) which coincides to the max of η^*, i.e. around 26 %. Therefore, by optimizing the geometry and by adding a periodic grating at the rear side layer, we were able to enhance light absorption and current density. As shown in the previous sections, the geometry of the Schottky cell is well-suited for the plasmonic enhancement (of the photo-generation process), since the metal grating can be used both as a contact and a junction (Schottky barrier). In these calculations, the used absorber was Silicon, and thanks to the bifacial configuration (that allows for light collection from both sides of the SC), 85% enhancement in short circuit current was achieved, despite the low absorption coefficient of Si.

4. Conclusion

We performed numerical investigations for ultra-thin Schottky bifacial photovoltaic solar cells coupled to (periodic) plasmonic gratings for highly-efficient light trapping and confinement. We have demonstrated that using bifacial design, i.e. collecting light from both facets of the cell,an impressive 88% enhancement of the short-circuit current can be achieved with a bifaciality factor of 84%. This results in a normalized efficiency of 25% that significantly exceeds the 15% efficiency achieved in monofacial Schottky SC[22].

The observed enhancement is akin to the peculiar characteristics of plasmonic arrays, that result in strong photonic scattering, which increases the coupling into the Si (thin film) layer, at both faces. Finally, due to its simplicity, the SC design proposed here can be realized experimentally quite easily and will help increase the efficiency and reduce the cost of Schottky-based PV devices.

Acknowledgment

AAB Baloch and SN Rashkeev would like to thank the Qatar National Research Fund (QNRF) for supporting this project through the National Priorities Research Program (NPRP) Exceptional grant, NPRP X-107-1-027. Also, FH Alharbi would like to thank the King Abdullah City for Atomic and Renewable Energy (K.A.CARE) for providing funding support.

Conflict of Interest

The authors declare that they have no known financial/commercial conflict of interest.

References

[1] Timilsina Govinda R, Kurdgelashvili Lado, Narbel Patrick A. Solar energy: Markets, economics and policies. *Renewable and sustainable energy reviews.* **2012**,16(1),449–465.

[2] Devabhaktuni Vijay, Alam Mansoor, Depuru Soma Shekara Sreenadh Reddy, Green II Robert C, Nims Douglas, Near Craig. Solar energy: Trends and enabling technologies. *Renewable and Sustainable Energy Reviews.* **2013**,19,555–564.

[3] Friedrichs Jörg. Global energy crunch: How different parts of the world would react to a peak oil scenario. *Energy policy.* **2010**,38(8),4562–4569.

[4] Sorrell Steve, Speirs Jamie, Bentley Roger, Brandt Adam, Miller Richard. Global oil depletion: A review of the evidence. *Energy Policy.* **2010**,38(9),5290–5295.

[5] Mudd Gavin M, Diesendorf Mark. Sustainability of uranium mining and milling: toward quantifying resources and eco-efficiency. *Environmental Science & Technology.* **2008**,42(7),2624–2630.

[6] Ghosh Arindam, Krishnan Yamuna. At a long-awaited turning point. *Nature nanotechnology.* **2014**,9(7),491.

[7] Gorjiara T, Baldock Clive. Nanoscience and nanotechnology research publications: a comparison between Australia and the rest of the world. *Scientometrics.* **2014**,100(1),121–148.

[8] Green Martin A. Silicon photovoltaic modules: a brief history of the first 50 years. *Progress in Photovoltaics: Research and applications.* **2005**,13(5),447–455.

[9] Goetzberger Adolf, Hebling Christopher, Schock Hans-Werner. Photovoltaic materials, history, status and outlook. *Materials Science and Engineering: R: Reports.* **2003**,40(1),1–46.

[10] Alharbi Fahhad, Bass John D, Salhi Abdelmajid, Alyamani Ahmed, Kim Ho-Cheol, Miller Robert D. Abundant non-toxic materials for thin film solar cells: Alternative to conventional materials. *Renewable Energy.* **2011**,36(10),2753–2758.

[11] Kojima Akihiro, Teshima Kenjiro, Shirai Yasuo, Miyasaka Tsutomu. Organometal halide perovskites as visible-light sensitizers for photovoltaic cells. *Journal of the American Chemical Society.* **2009**,131(17),6050–6051.

[12] *National Renewable Energy Laboratory, Best Research-Cell Efficiency Chart, https://www.nrel.gov/pv/cell-efficiency.html (accessed: December 2019).* **2019**.

[13] Baloch Ahmer AB, Hossain MI, Tabet N, Alharbi FH. *Practical Efficiency Limit of Methylammonium Lead Iodide Perovskite Solar Cells, Journal of Physical Chemistry Letters.* **2018**.

[14] El-Mellouhi Fedwa, Bentria El Tayeb, Rashkeev Sergey N, Kais Sabre, Alharbi Fahhad H. Enhancing intrinsic stability of hybrid perovskite solar cell by strong, yet balanced, electronic coupling. *Scientific reports.* **2016**,6,30305.

[15] Nelson Jenny. *The physics of solar cells*. World Scientific Publishing Company; **2003**.

[16] Wurfel P. *Physics of Solar Cells. Willey.* **2005**.

[17] Catchpole KR, , Polman Albert. Plasmonic solar cells. *Optics express.* **2008**,16(26),21793–21800.

[18] Nakayama Keisuke, Tanabe Katsuaki, Atwater Harry A. Plasmonic nanoparticle enhanced light absorption in GaAs solar cells. *Applied Physics Letters.* **2008**,93(12),121904.

[19] Ferry Vivian E, Verschuuren Marc A, Li Hongbo BT, et al. Light trapping in ultrathin plasmonic solar cells. *Optics express.* **2010**,18(102),A237–A245.

[20] Green Martin A, Pillai Supriya. Harnessing plasmonics for solar cells. *Nature Photonics.* **2012**,6(3),130.

[21] Atwater Harry A, Polman Albert. Plasmonics for improved photovoltaic devices. In: World Scientific **2011** (pp. 1–11).

[22] Farhat M, Kais S, Alharbi FH. Plasmonically enhanced Schottky photovoltaic devices. *Scientific reports.* **2017**,7(1),14253.

[23] Maier Stefan Alexander. *Plasmonics: fundamentals and applications*. Springer Science & Business Media; **2007**.

[24] Alaee Rasoul, Farhat Mohamed, Rockstuhl Carsten, Lederer Falk. A perfect absorber made of a graphene micro-ribbon metamaterial. *Optics express.* **2012**,20(27),28017–28024.

[25] Thongrattanasiri Sukosin, Koppens Frank HL, De Abajo F Javier Garcia. Complete optical absorption in periodically patterned graphene. *Physical review letters.* **2012**,108(4),047401.

[26] Chen Pai-Yen, Farhat Mohamed, Bağc Hakan. Graphene metascreen for designing compact

infrared absorbers with enhanced bandwidth. *Nanotechnology.* **2015**,26(16),164002.

[27] Chen Pai-Yen, Argyropoulos Christos, Farhat Mohamed, Gomez-Diaz J Sebastian. Flatland plasmonics and nanophotonics based on graphene and beyond. *Nanophotonics.* **2017**,6(6),1239–1262.

[28] Kim Seyoon, Jang Min Seok, Brar Victor W, Mauser Kelly W, Kim Laura, Atwater Harry A. Electronically tunable perfect absorption in graphene. *Nano letters.* **2018**,18(2),971–979.

[29] Molesky Sean, Dewalt Christopher J, Jacob Zubin. High temperature epsilon-near-zero and epsilon-near-pole metamaterial emitters for thermophotovoltaics. *Optics express.* **2013**,21(101),A96–A110.

[30] Aberle Armin G. Thin-film solar cells. *Thin solid films.* **2009**,517(17),4706–4710.

[31] Kraemer Daniel, Poudel Bed, Feng Hsien-Ping, et al. High-performance flat-panel solar thermoelectric generators with high thermal concentration. *Nature materials.* **2011**,10(7),532.

[32] Brongersma Mark L, Halas Naomi J, Nordlander Peter. Plasmon-induced hot carrier science and technology. *Nature nanotechnology.* **2015**,10(1),25.

[33] Lee Young Keun, Lee Hyosun, Lee Changhwan, Hwang Euyheon, Park Jeong Young. Hot-electron-based solar energy conversion with metal–semiconductor nanodiodes. *Journal of Physics: Condensed Matter.* **2016**,28(25),254006.

[34] Sakhdari Maryam, Hajizadegan Mehdi, Farhat Mohamed, Chen Pai-Yen. Efficient, broadband

and wide-angle hot-electron transduction using metal-semiconductor hyperbolic metamaterials. *Nano Energy.* **2016**,26,371–381.

[35] Hezel Rudolf. Recent progress in MIS solar cells. *Progress in Photovoltaics: Research and Applications.* **1997**,5(2),109–120.

[36] Godfrey RB, Green MA. 655 mV open-circuit voltage, 17.6% efficient silicon MIS solar cells. *Applied physics letters.* **1979**,34(11),790–793.

[37] Fan Guifeng, Zhu Hongwei, Wang Kunlin, et al. Graphene/silicon nanowire Schottky junction for enhanced light harvesting. *ACS applied materials & interfaces.* **2011**,3(3),721–725.

[38] Tong Chong, Yun Juhyung, Song Haomin, Gan Qiaoqiang, Anderson Wayne A. Plasmonic-enhanced Si Schottky barrier solar cells. *Solar Energy Materials and Solar Cells.* **2014**,120,591–595.

[39] Arquer F Pelayo Garca, Konstantatos Gerasimos. Metal-insulator-semiconductor heterostructures for plasmonic hot-carrier optoelectronics. *Optics express.* **2015**,23(11),14715–14723.

[40] Chatterjee Avigyan, Biswas Ashim Kumar, Sinha Amitabha. Dependence of the photocurrent of a schottky-barrier solar cell on the back surface recombination velocity and suggestion for a structure with improved performance. *Journal of Solar Energy.* **2015**,2015.

[41] Safir Yakov. *Bifacial solar cell.* US Patent 5,665,175; **1997**.

[42] Ohtsuka H, Sakamoto M, Tsutsui K, Yazawa Y. Bifacial silicon solar cells with 21. 3% front efficiency and 19. 8% rear efficiency. *Progress in Photovoltaics: Research and Applications.* **2000**,8(4),385–390.

[43] Russell Thomas CR, Saive Rebecca, Augusto André, Bowden Stuart G, Atwater Harry A. The influence of spectral albedo on bifacial solar cells: A theoretical and experimental study. *IEEE Journal of photovoltaics.* **2017**,7(6),1611–1618.

[44] Asadpour Reza, Chavali Raghu VK, Ryyan Khan M, Alam Muhammad A. Bifacial Si heterojunction-perovskite organic-inorganic tandem to produce highly efficient (η T* 33%) solar cell. *Applied Physics Letters.* **2015**,106(24),243902.

[45] Ryyan Khan M, Alam Muhammad A. Thermodynamic limit of bifacial double-junction tandem solar cells. *Applied Physics Letters.* **2015**,107(22),223502.

[46] Khan M Ryyan, Hanna Amir, Sun Xingshu, Alam Muhammad A. Vertical bifacial solar farms: Physics, design, and global optimization. *Applied energy.* **2017**,206,240–248.

[47] Guerrero-Lemus R, Vega R, Kim Taehyeon, Kimm Amy, Shephard LE. Bifacial solar photovoltaics–A technology review. *Renewable and sustainable energy reviews.* **2016**,60,1533–1549.

[48] Baldridge Alice M, Hook SJ, Grove CI, Rivera G. The ASTER spectral library version 2.0. *Remote Sensing of Environment.* **2009**,113(4),711–715.

[49] Multiphysics COMSOL. *Reference Manual v. 5.2. COMSOL AB, Stockholm, Sweden.* **2017**.

[50] Aspnes David E, Studna AA. Dielectric functions and optical parameters of si, ge, gap, gaas, gasb, inp, inas, and insb from 1.5 to 6.0 ev. *Physical review B.* **1983**,27(2),985.

[51] Rakić Aleksandar D, Djurišić Aleksandra B, Elazar Jovan M, Majewski Marian L. Optical properties of metallic films for vertical-cavity optoelectronic devices. *Applied optics.* **1998**,37(22),5271–5283.

[52] Boroumand Javaneh, Das Sonali, Vázquez-Guardado Abraham, Franklin Daniel, Chanda Debashis. Unified electromagnetic-electronic design of light trapping silicon solar cells. *Scientific reports.* **2016**,6,31013.

[53] Farhat Mohamed, Cheng Tsung-Chieh, Le Khai Q, Cheng Mark Ming-Cheng, Bağc Hakan, Chen Pai-Yen. Mirror-backed dark alumina: a nearly perfect absorber for thermoelectronics and thermophotovotaics. *Scientific reports.* **2016**,6,19984.

Table of Contents Entry

Synergistic effect of plasmonic materials and bifaciality was investigated for a Schottky junction solar cell using a coupled opto-electronic model. By optimizing the geometry of the front and rear plasmonic gratings,photocarrier generation was improved by 88%. Optimal filling fractions corresponded to (0.5,0.5) for a normalized efficiency of 25%.

Keywords: Plasmonics, Schottky,Bifacial,Photovoltaic,Optoelectronic.

Authors: M. Farhat, A. A. B. Baloch, S. Rashkeev, N. Tabet, S. Kais, Fahhad H. Alharbi

Title: Bifacial Schottky-Junction Plasmonic-based Solar Cell

TOC Figure:

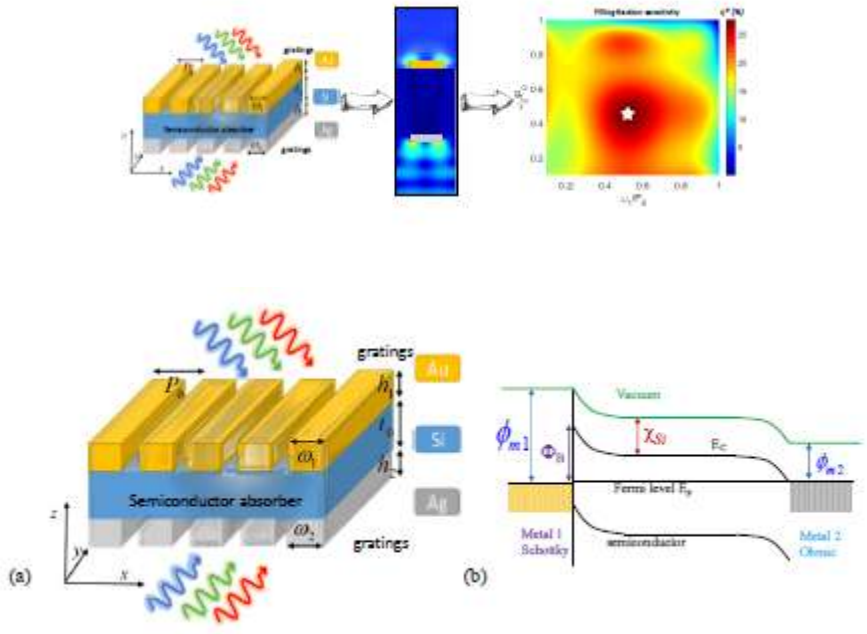

Figure 1: (a) Schematic of the proposed bifacial Schottky solar cell with a gold grating on top and a silver grating on the bottom, and a silicon absorber. The geometrical parameters of the structure are: the period of the grating is P_0 , h_1 and h_2 are the grating heights, the thickness of the absorber is t_0 , and ω_1 / P_0 and ω_2 / P_0 are the filling fractions of front and rear faces, respectively.(b) Schematic of the Band bending in a Schottky-based solar cell.

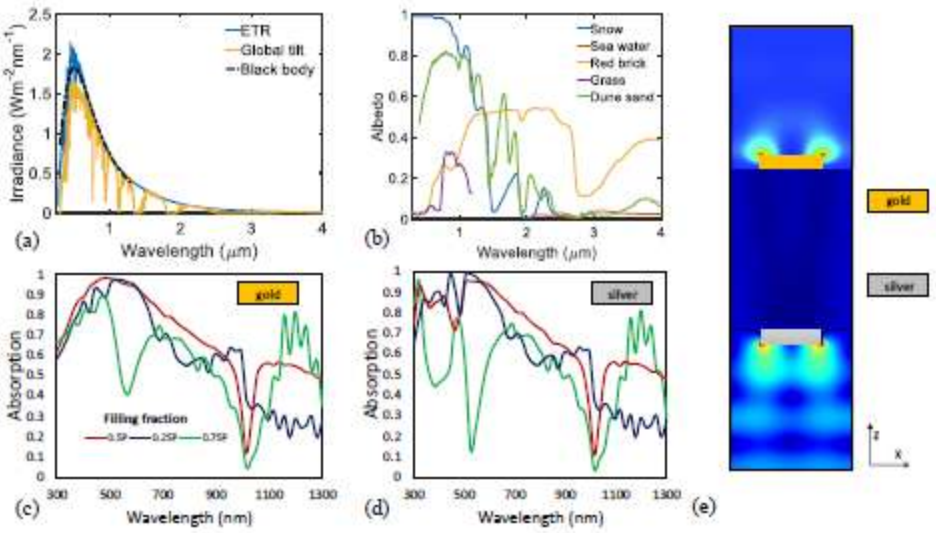

Figure 2: (a) Extraterrestrial radiation (ETR) (blue line) and global tilt (yellow line) solar spectral irradiance versus wavelength of light in μ m, compared to the black body radiation at 5800 K, as given by Eq. (7). (b) Albedo coefficient for different materials as taken from the measurements[48]. (c) Absorption spectrum from the direct light irradiation (given in Figure 2(a)) for different filling fraction of the gratings ω_i / P_0 (0.25, 0.5, and 0.75). (d) Absorption spectrum from the albedo light irradiation [given in Figure 2(b)]. (e) Electric field norm profile in the bifacial solar cell when using gold and silver as front and back electrodes of heights 100 nm, each and filling fraction of 0.5, as well as $t_0 = 3$ μ m, respectively. Higher value of the electric field corresponds to lighter colors in the figure.

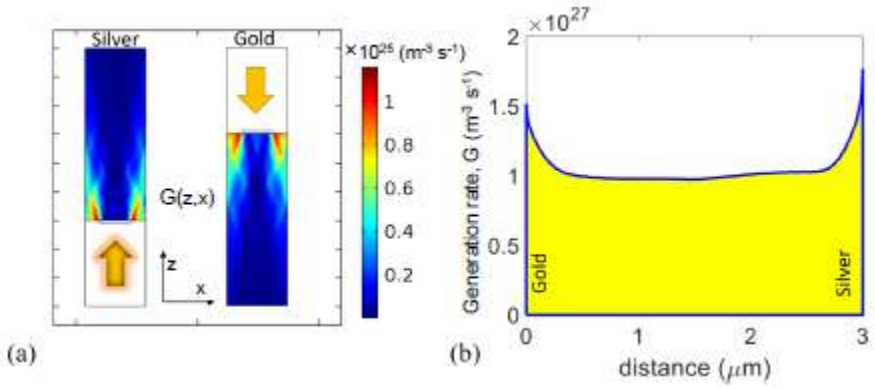

Figure 3: (a) Spectral Generation ($G((\mathbf{r})$) profile inside the silicon layer with both gratings considered (left: silver and right: gold). (b) Total spectrally-integrated generation of the bifacial

Schottky solar cell along the z-axis.

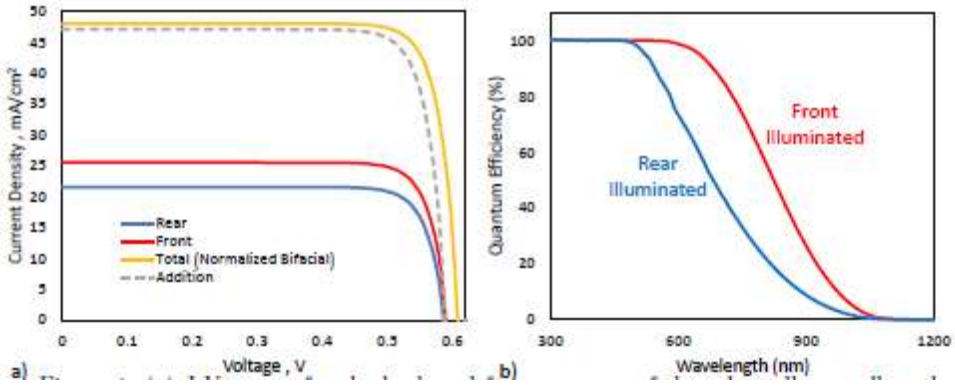

Figure 4: (a) J-V curves for the back and front contacts of the solar cell, as well as the total one, resulting from the generation profile given in Fig. 3(b). (b) Internal quantum efficiency for the front and back illuminated contacts.

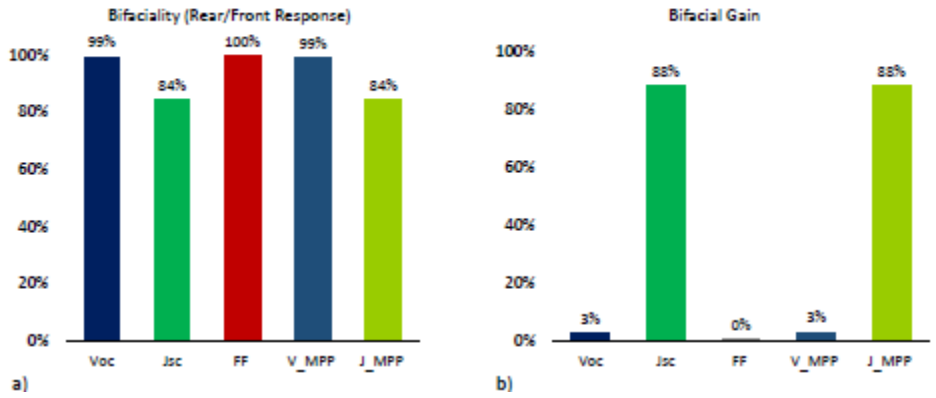

Figure 5: (a) Bifaciality factor (rear to front response) of Schottky solar cells for key electrical parameters (b) Bifacial gain as a result of illuminating device from both sides of cell.Here, subscript MPP denotes maximum power point, oc is open circuit and sc is short circuit condition

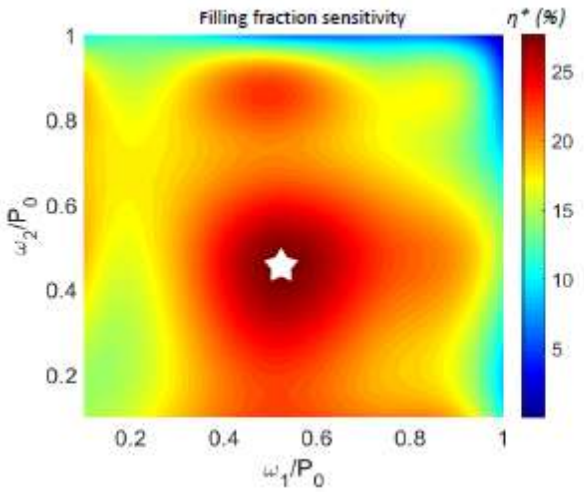

Figure 6: Modified normalized output η^* of the PV cell as a function of the filling fractions of the plasmonic gratings (ω_1 / P_0 and ω_2 / P_0).